Structure and activity of the only human RNase T2: Supplementary material

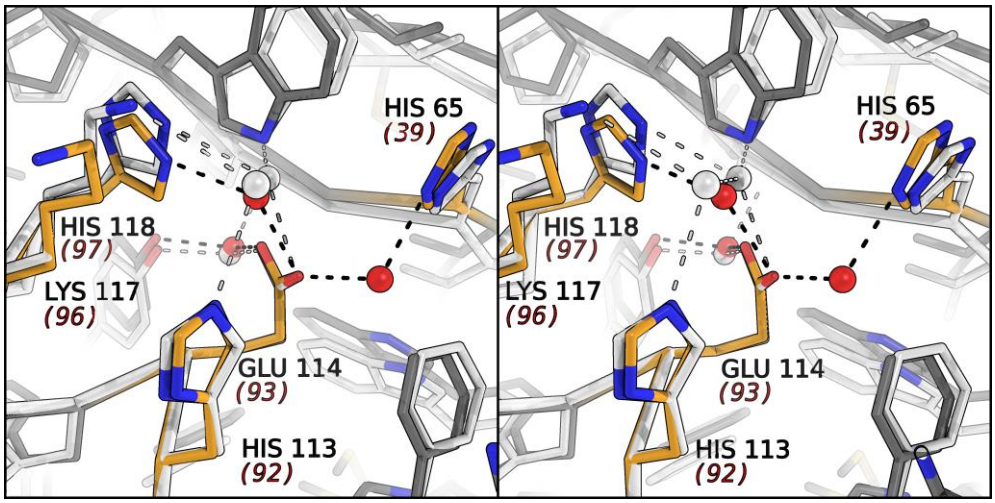

Supplementary Figure 1: Overlay of the active sites of RNase LE and RNase T2. Here, the active site of RNase LE [PDB 1DIX, 1] is shown in white, while human RNase T2 is shown in gray and yellow (catalytic residues) with white and red H_2O oxygen atoms as spheres, respectively. The numbers in brackets refer to the residues numbers in PDB entry 1DIX. The active site of human RNase T2 shows much similarity with other enzymes in this family, and hence the same catalytic can be assumed (see Supplementary Fig. 2).

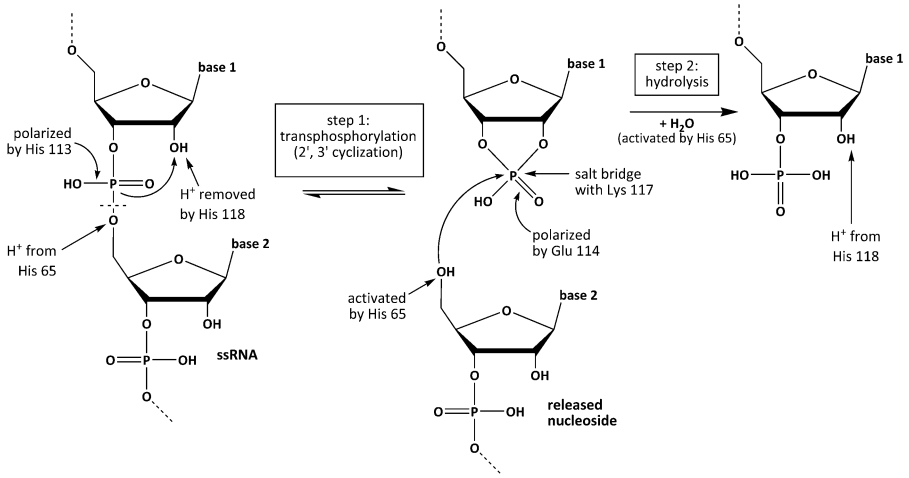

Supplementary Figure 2: Assumed reaction mechanism. The assumed reaction mechanism for human RNase T2 analogous [2] is specific for RNA as opposed to DNA. The cleavage of the phosphodiester bond consists of two steps, transphosphorylation and hydrolysis. In the first step, the phosphate group of the single-stranded RNA to be cleaved is polarized by His 113, while His 118 as base catalyst removes a proton from the 2'OH group of the ribose [3] as base catalyst. The positively polarized phosphorous atom is attacked by the nucleophilic 2'-oxygen to form a five-membered ring, which is stabilized by Glu 114 and trough a salt bridge to Lys 117. For the hydrolysis step, His 65 is assumed to activate a water molecule and the hydroxyl group of the ribose, which then attacks the P-O group and forms the 3' nucleotide ring, as the product is re-protonated by His 118 [3].

Supplementary Table 1: Summary of the collection statistics for anomalous data.

Source	BESSY MX 14.1
Unit cell dimensions	a = 31.328 Å, b = 68.146 Å, c = 47.990 Å, β = 90.827°
Space group	$P2_1$
Wavelength (Å)	1.950
Oscillation range	95°
Resolution range (Å)	47.90–2.23 (2.33–2.23)
No. of observations	68336 (6068)
Unique*	18256 (1919)
Redundancy*	3.58 (2.54)
Completeness* (%)	95.5 (80.2)
Mean I/σ(I)	13.66 (1.98)
R_{int} (%)	8.00 (49.44)
R_{rim} (%)	9.39 (58.24)
R_{pim} (%)	3.47 (22.98)
R_{anom} (%)	8.33 (66.99)
<|ΔF|/σ(ΔF)>	0.88 (0.87)

Values in parentheses refer to outer shell.
*Friedel pairs not merged.

Tandem mass spectrometry for N-glycopeptides in RNaseT2

Methods. RNaseT2 protein was reduced with 50mM DTT for 1 h at 37°C, alkylated with 100mM IAA for 1h at 37°C and digested with modified trypsin (Promega) overnight at 37 °C. Tryptic peptides were injected into a C18 precolumn (1.5 cm, 360 µm o.d., 150 µm i.d., Reprosil-Pur 120 Å, 3 µm, C18-AQ, Dr. Maisch GmbH) at a flow rate of 10 mL/min. Bound peptides were eluted and separated on a C18 capillary column (15 cm, 360 µm o.d., 75 µm i.d., Reprosil-Pur 120 Å, 3 µm, C18-AQ, Dr. Maisch GmbH) at a flow rate of 300 µL/min, with a gradient from 7.5 to 37.5% ACN in 0.1% formic acid for 60 min using an Agilent 1100 nano-flow LC system (Agilent Technologies) coupled to an LTQ-Orbitrap Velos hybrid mass spectrometer (Thermo Fisher Scientific). Mass spectrometry conditions were: spray voltage, 1.6 kV; heated capillary temperature, 270 °C; normalized higher energy collision dissociation (HCD) with collision energy 42.5 % for MS/MS in a HCD collision cell. The mass spectrometer was operated in data-dependent mode to automatically switch between MS and MS/MS acquisition. Survey MS spectra were acquired in the orbitrap (m/z 350–1600) with the resolution set to 30,000 at m/z 400 and automatic gain control target at $5x10^5$. The ten most intense ions were sequentially isolated for HCD MS/MS fragmentation and detection in the orbitrap. Ions with single and unrecognized charge states were excluded. For all measurements with the orbitrap detector a lock-mass ion from ambient air (m/z 445.120025) was used for internal calibration. Raw data were analyzed with Mascot search engine for peptide and protein identifications (Version 2.2.07, Matrix Science). SwissProt human database was used as sequence database. The MS mass tolerance was set to 10 ppm and MS/MS mass tolerance was set to 0.1 Da. Up to three missed cleavages of trypsin were allowed. Oxidized methionine, cysteine carbamido-methylation and asparagine HexNAc were searched as variable modifications.

Results

Sequence	Modification	Exp. m/z	Exp. M.W.	Charge	Cal. M.W.	Error (ppm)	Score
SEGC**N**R	Cam (C), Hex (N)	463.1879	924.3612	2	924.3607	0.58	10.9

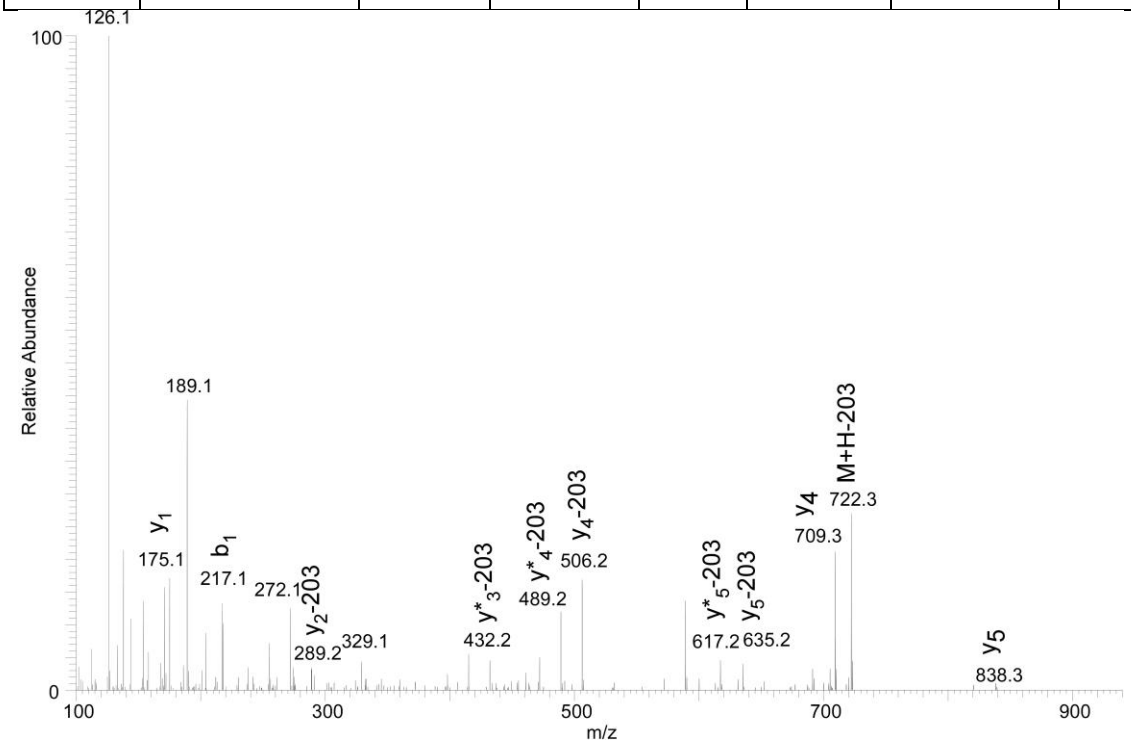

#	b	b^{++}	b*	b^{*++}	b^{0}	b^{0++}	Seq.	y	y^{++}	y*	y^{*++}	y^{0}	y^{0++}	#
1	88.0393	44.5233			70.0287	35.5180	S							6
2	**217.0819**	109.0446			199.0713	100.0393	E	**635.2566**	318.1319	**618.2300**	309.6187	**617.2460**	309.1267	5
3	**274.1034**	**137.5553**			256.0928	128.5500	G	**506.2140**	253.6106	**489.1875**	245.0974			4
4	434.1340	**217.5706**			416.1235	208.5654	C	**449.1925**	225.0999	**432.1660**	**216.5866**			3
5	548.1769	**274.5921**	**531.1504**	266.0788	530.1664	265.5868	N	**289.1619**	145.0846	**272.1353**	136.5713			2
6							R	**175.1190**	88.0631	158.0924	79.5498			1

Sequence	Modification	Exp. m/z	Exp. M.W.	Charge	Cal. M.W.	Error (ppm)	Score
AYWPDVIHSFP**N**R	Hex (N)	451.9725	1803.8609	4	1803.8580	1.58	18.5

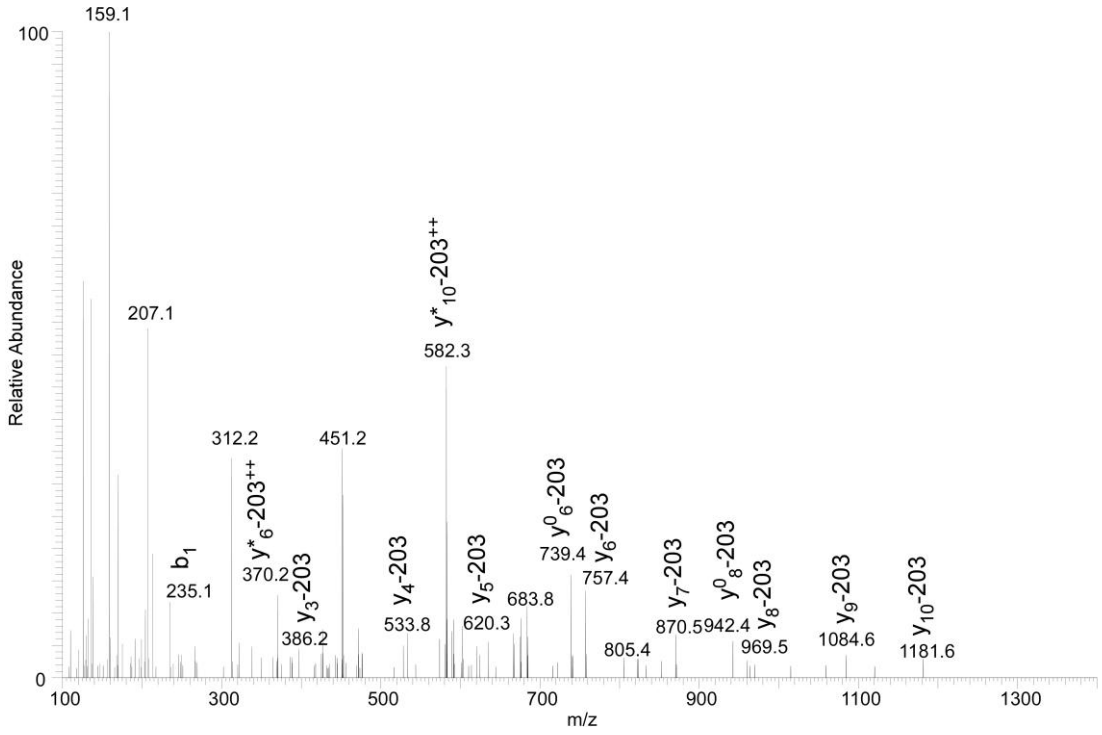

#	b	b^{++}	b*	b*$^{++}$	b^{0}	b^{0++}	Seq.	y	y^{++}	y*	y*$^{++}$	y^{0}	y^{0++}	#
1	72.0444	36.5258					A							13
2	**235.1077**	118.0575					Y	1530.7488	765.8781	1513.7223	**757.3648**	1512.7383	**756.8728**	12
3	421.1870	211.0972					W	1367.6855	**684.3464**	1350.6589	**675.8331**	1349.6749	**675.3411**	11
4	518.2398	259.6235					P	**1181.6062**	**591.3067**	1164.5796	**582.7935**	**1163.5956**	**582.3014**	10
5	633.2667	317.1370			615.2562	308.1317	D	**1084.5534**	542.7803	1067.5269	**534.2671**	1066.5429	**533.7751**	9
6	732.3352	366.6712			714.3246	357.6659	V	**969.5265**	485.2669	952.4999	**476.7536**	951.5159	**476.2616**	8
7	845.4192	423.2132			827.4087	414.2080	I	**870.4581**	435.7327	853.4315	**427.2194**	**852.4475**	**426.7274**	7
8	982.4781	491.7427			**964.4676**	482.7374	H	**757.3740**	379.1906	**740.3475**	**370.6774**	**739.3634**	**370.1854**	6
9	1069.5102	535.2587			1051.4996	526.2534	S	**620.3151**	310.6612	603.2885	302.1479	**602.3045**	301.6559	5
10	1216.5786	608.7929			1198.5680	599.7876	F	**533.2831**	**267.1452**	516.2565	258.6319			4

11	1313.6313	657.3193			1295.6208	648.3140	P	386.2146	193.6110	369.1881	185.0977			3
12	1427.6743	714.3408	1410.6477	705.8275	1409.6637	705.3355	N	289.1619	145.0846	272.1353	136.5713			2
13							R	175.1190	88.0631	158.0924	79.5498			1

Sequence	Modification	Exp. m/z	Exp. M.W.	Charge	Cal. M.W.	Error (ppm)	Score
QDQQLQNCTEPGEQPSPK	Cam (C), Hex (N)	763.0073	2286.0001	3	2286.0070	-3.04	30.6

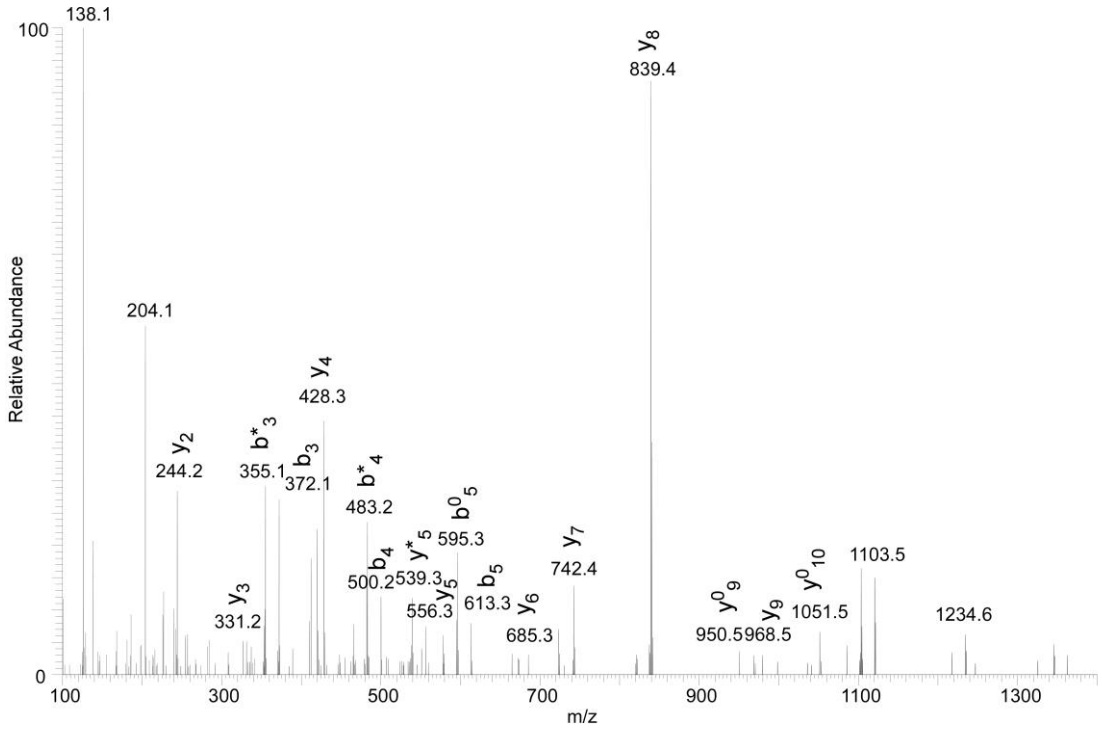

#	b	b^{++}	b*	b^{*++}	b^0	b^{0++}	Seq.	y	y^{++}	y*	y^{*++}	y^0	y^{0++}	#
1	129.0659	65.0366	112.0393	56.5233			Q							18
2	244.0928	122.5500	227.0662	114.0368	226.0822	113.5448	D	1955.8764	978.4418	1938.8498	969.9285	1937.8658	969.4365	17
3	372.1514	186.5793	355.1248	178.0661	354.1408	177.5740	Q	1840.8494	920.9283	1823.8229	912.4151	1822.8388	911.9231	16
4	500.2100	250.6086	483.1834	242.0953	482.1994	241.6033	Q	1712.7908	856.8991	1695.7643	848.3858	1694.7803	847.8938	15
5	613.2940	307.1506	596.2675	298.6374	595.2835	298.1454	L	1584.7323	792.8698	1567.7057	784.3565	1566.7217	783.8645	14
6	741.3526	371.1799	724.3260	362.6667	723.3420	362.1747	Q	1471.6482	736.3277	1454.6216	727.8145	1453.6376	727.3225	13

7	855.3955	428.2014	838.3690	419.6881	837.3850	419.1961	N	1343.5896	672.2984	1326.5631	663.7852	1325.5791	663.2932	12
8	1015.4262	508.2167	998.3996	499.7035	997.4156	499.2114	C	1229.5467	615.2770	1212.5201	606.7637	1211.5361	606.2717	11
9	1116.4739	558.7406	1099.4473	550.2273	1098.4633	549.7353	T	1069.5160	535.2617	1052.4895	526.7484	1051.5055	526.2564	10
10	1245.5165	623.2619	1228.4899	614.7486	1227.5059	614.2566	E	968.4684	484.7378	951.4418	476.2245	950.4578	475.7325	9
11	1342.5692	671.7882	1325.5427	663.2750	1324.5587	662.7830	P	839.4258	420.2165	822.3992	411.7032	821.4152	411.2112	8
12	1399.5907	700.2990	1382.5641	691.7857	1381.5801	691.2937	G	742.3730	371.6901	725.3464	363.1769	724.3624	362.6849	7
13	1528.6333	764.8203	1511.6067	756.3070	1510.6227	755.8150	E	685.3515	343.1794	668.3250	334.6661	667.3410	334.1741	6
14	1656.6919	828.8496	1639.6653	820.3363	1638.6813	819.8443	Q	556.3089	278.6581	539.2824	270.1448	538.2984	269.6528	5
15	1753.7446	877.3759	1736.7181	868.8627	1735.7340	868.3707	P	428.2504	214.6288	411.2238	206.1155	410.2398	205.6235	4
16	1840.7766	920.8920	1823.7501	912.3787	1822.7661	911.8867	S	331.1976	166.1024	314.1710	157.5892	313.1870	157.0972	3
17	1937.8294	969.4183	1920.8029	960.9051	1919.8188	960.4131	P	244.1656	122.5864	227.1390	114.0731			2
18							K	147.1128	74.0600	130.0863	65.5468			1

REFERENCES

1. Tanaka, N., Arai, J., Inokuchi, N., Koyama, T., Ohgi, K., Irie, M. and Nakamura, K.T. (2000) Crystal structure of a plant ribonuclease, RNase LE. *J Mol Biol*, **298**, 859-873.
2. Kurihara, H., Nonaka, T., Mitsui, Y., Ohgi, K., Irie, M. and Nakamura, K.T. (1996) The crystal structure of ribonuclease Rh from Rhizopus niveus at 2.0 A resolution. *J Mol Biol*, **255**, 310-320.
3. Deshpande, R.A. and Shankar, V. (2002) Ribonucleases from T2 family. *Crit Rev Microbiol*, **28**, 79-122.